Int. J. Electrochem. Sci., 10 **(2015)** 5327 - 5337

International Journal of
ELECTROCHEMICAL
SCIENCE
www.electrochemsci.org

Preparation of Ultrafine Barium Titanate under Wet Chemical Mixing Method with $TiOSO_4$. Sintering Performance and Dielectric Properties

Wenwei Chi[1], *Dali Zhou*[1,*], *Yi Xia*[1,2], *Jiabei Zhou*[1], *Si Sun*[1]

[1]Department of Materials Science and Engineering, Sichuan University, Chengdu 610064, PR China
[2]Rsearch Center for Analysis and Measurement, Kunming University of Science and Technology, Kunming 650224, China
[*]E-mail: chiwenweiwork@163.com; zdl@scu.edu.cn

Received: 28 March 2015 / *Accepted:* 30 April 2015 / *Published:* 27 May 2015

Using neutralized-hydrolysis and self-dissociate products of $TiOSO_4$ as Ti sources respectively, the synthesis of ultra-fine barium titanate ($BaTiO_3$) powders under wet chemical mixing-calcining process was studied. The structure of $BaTiO_3$ powders were characterized by XRD, TG/DTG, ICP, Raman and SEM analysis. The powders were sintered into ceramics and the dielectric properties of the ceramics were also investigated by LCR meter. The results indicated that alcohol as $BaCO_3$ crystal growth inhibitor promotes the formation of uniform precursors. Neutralized-hydrolysis products are more suitable for the production of fine $BaTiO_3$ powders than self-dissociate products. Pure cubic phase $BaTiO_3$ powders with average particle size 90 nm were synthesized after two hours calcinations at 700 °C. Tetragonal phase $BaTiO_3$ powders prepared at 900 °C can be sintered into ceramics at 1230 °C with relative density 96.1%.The ceramic sintered at 1260 °C showed the best dielectric properties with average grain size 0.95 nm.

Keywords: Powders; $BaTiO_3$; Wet chemical mixing; $TiOSO_4$

1. INTRODUCTION

The traditional industrial process of $BaTiO_3$ powders is solid-state reaction [1-3]. According to the phase evolution of solid-state $BaTiO_3$ studies [1,4,5], initial TiO_2 powders' size and morphology have a significant impact on the size and shape of the $BaTiO_3$ particles. Because $BaTiO_3$ formation is dominated by the Ba^{2+} diffusion rate through the perovskite layer which is formed at the contact points between $BaCO_3$ and TiO_2 at the beginning of reaction. To shorten the diffusion distance, promote the reaction and lower the calcination temperature, good homogeneity of the mixture composed of ultrafine submicron-size reactants is desired. However, the preferential growth direction of $BaCO_3$ is (100), so it usually presents noodle shape with length-to-diameter ratio more than 10. Thus good homogeneity of the mixture rely on long-term intensive ball-milling this goal on certain level [6, 7]. However, undesired contaminations from the milling media and energy consumption inevitably rise. Hydrolysis of $TiOSO_4$ includes self-dissociate at boiling temperature and neutralized-hydrolysis. Self-dissociate at boiling temperature is intermediate step of production of TiO_2. Neutralized-hydrolysis product made by chloride or sulphate solutions of titanium with addition of aqueous solution of ammonia or sodium hydroxide at room temperature is amorphous phase. The product transforms into ultrafine TiO_2 nanoparticles with average diameter less than 10 nm after calcinations [8-10]. In addition, randomly oriented 2–5 nm anatase crystals embedded in amorphous product in the procedure of calcinations can be observed by TEM [8].Using hydrolysis products of $TiOSO_4$ as Ti source has never been investigated in solid reaction preparation $BaTiO_3$ before. Some organic solvents can be used to suppress crystal growth in preparation of nanoparticles. So during the reaction $CO_3^{2-}+Ba^{2+}\rightarrow BaCO_3$, finer $BaCO_3$ can be produced by adding organic solvents in solvent.

In this research, wet chemical mixing process is proposed to replace traditional ball-milling. Because of the low price, two kinds of hydrolysis products of $TiOSO_4$ were used as Ti source after washing away SO_4^{2-}. $BaCO_3$ is generated by the reaction between $BaCl_2$ and $(NH_4)_2CO_3$ during the mixing process. This method allows for precursors with good mixing uniformity by addition alcohol in the solvent as crystal growth inhibitor. The $BaTiO_3$ powders sintering performance and dielectric properties were also investigated.

2. EXPERIMENT

2.1. Starting Reagents and Synthesis

All reactants of analytical grade ($BaCl_2•2H_2O$, 99.5%, $TiOSO_4$, 92%, Ltd. $NH_4•H_2O$, 28% , $(NH_4)_2CO_3$, 99%, C_2H_5OH,99.9%，all provided by Tianjin Fine Chemical Co.) were used without further purification. 12.8 g $TiOSO_4$ was dissolved in 128 ml water by keeping the temperature of water bath at 75 ^oC under stirring. To get different hydrolysis products, $TiOSO_4$ solutions pH was then adjusted to 9.0 by rapidly adding ammonium hydroxide under vigorously stirring or heated to boiling temperature both resulting in white precipitates. The white precipitates obtained were separated by filtration and sulphate ions were washed (as was confirmed by the $BaCl_2$ test) with distilled water and ammonium hydroxide. The Ti sources were further dispersed in 250 ml distilled water or alcohol solvent composed of certain amount alcohol and distilled water, then mixed with certain amount of $BaCl_2$. $BaCl_2$ in mixture was precipitated by adding the mixed solution of $NH_3·H_2O$ and $(NH_4)_2CO_3$. The precursor was separated by filtration and vacuum dried at room temperature. The dried precursors were further calcined in air at designed temperature for certain time. After calcination, the ceramic powders mixed with suitable amount binder in agate mortar were pressed into discs of 15 mm in diameter and 1 mm in thickness. The pressed discs were sintered at different temperatures for 2 hours with a heating rate of 3 ^{o}C /min and the sintered pellets were polished and electroded with silver paste. The samples using neutralized-hydrolysis and self-dissociate products of $TiOSO_4$ were named as A and B respectively.

2.2. Characterization

To investigate the structural characteristics and phase purity of the synthesized $BaTiO_3$ nano-powders, X-ray diffract meter (XRD; DX-1000, Dangdong Fangyuan Instrument Co., Ltd, China) with CuKα radiation (k =0.15418 nm) operating at 40 kV and 25 mA was used. The diffraction pattern was scanned from 10 ^{o}C to 80 ^{o}C with speed of 2 ^{o}C /min. The unit cell parameters were determined by Rietveld analysis of the XRD patterns. The morphology and size of the synthesized $BaTiO_3$ particles were observed by field emission scanning electron microscopy (FE-SEM, Hitachi S4800) employing an accelerating voltage of 5 kV. The residual sulphate ions (SO_4^{2-}) content of the Ti sources washing free of sulphate ions was measured using inductively coupled plasma (ICP). Raman spectra were recorded in the 100−1100 cm^{-1} wave number range using a Raman microscope (Horiba Scientific). Laser radiation of 514 nm wavelength was employed as the excitation source. The absolute accuracy of Raman shifts was estimated to be ±0.2 cm^{-1} and all spectra were recorded at 25 ^{o}C under air. Simultaneous thermo gravimetric analysis (TG) (STA-449C, Netzsch, Germany) in air using an alumina crucible with a constant heating rate (10 ^{o}C /min) was used to investigate their kinetic reactions. Archimedes principle was employed to measure ceramics density. To examine the temperature dependence of the dielectric constants (ε) and dielectric loss of sintered pellets, measurements were carried out by Agilent E4980A precision LCR meter with a thermostat from 15 ^{o}C to 185 ^{o}C (heating rate 2 ^{o}C /min) at a frequency of 10 kHz. The dielectric constants was calculated by the equation:

$$\varepsilon=C*d/\varepsilon_0 S$$

where C is the capacitance of the sample examined by LCR meter, d is the thickness of the sample (m), ε_0=8.854 F/m is the vacuum permittivity and S is the cross section area (m^2).

3. RESULT AND DISCUSSION

3.1. Analysis of precursors

Fig .1(a) shows that the morphology of the $TiOSO_4$ neutralized-hydrolysis product. The product forms in irregular shape and aggregates with uniform size distribution about 50 nm in diameter, even smaller particles appeared after dried. It can be seen that solvent composition affects the precursors uniformity and the morphology of $BaCO_3$ for comparison of Fig .1(b) and (c). $BaCO_3$ forms aggregates composed of large-bar shape particles with long axis more than 2 μm and short axis about 200 nm in Fig .6(b). Alcohol in solvent restrains the growth of $BaCO_3$ and prevents forming aggregates. In Fig .1(c), $BaCO_3$ particles are worm-like shape with long axis less than 200 nm and short axis 40 nm. The finer $BaCO_3$ particles size close to the size of Ti source makes it is easier to achieve the homogeneous mixing goal [11]. In Fig. 1(d), $BaCO_3$ particles and self-dissociate products of $TiOSO_4$ can't be distinguished and some aggregates forms in local area. $BaCO_3$ morphology is not the restriction on forming uniform precursor, because there are no large bar-shape $BaCO_3$ particles as Fig .1(b) shows. The dispersancy of $TiOSO_4$ self–dissociate product's in alcohol solvent is worse than $TiOSO_4$ neutralized-hydrolysis product. The function Alcohol in solvent is still efficient on producing uniform precursor if the Ti source is self-dissociate products.

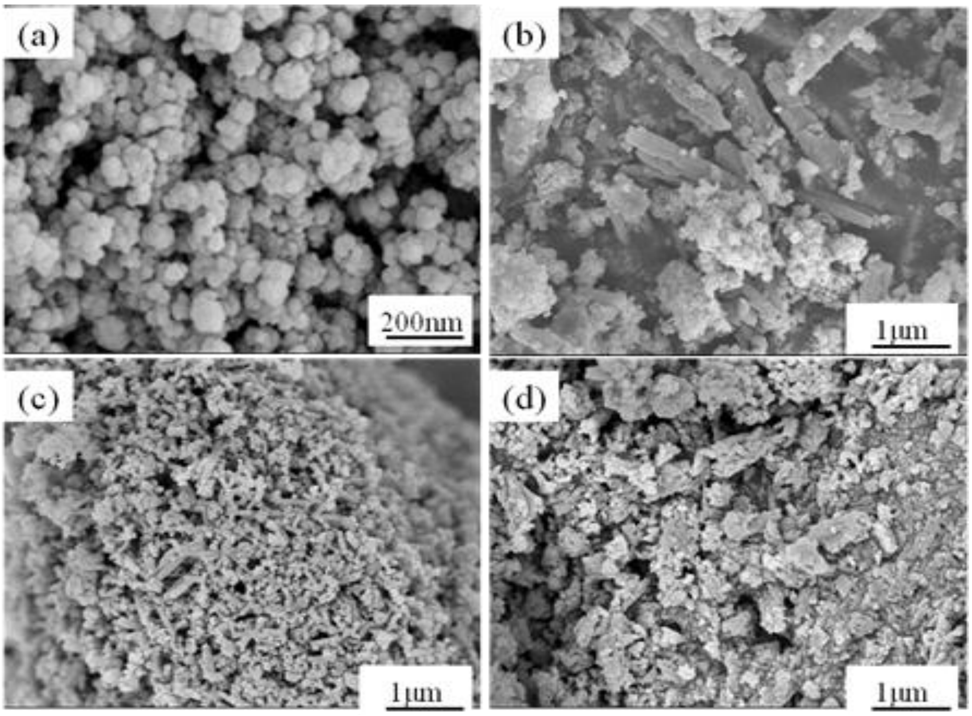

Figure 1. SEM micrographs of precusors (a) neutralized-hydrolysis product of $TiOSO_4$(b)precusor A synthsised in water (c) precusor A synthsised in alcohol solvent (d) precusor B synthsised in alcohol solvent.

3.2. Analysis of calcinations

Fig. 2 presents the TG and DTG graphs of precursors of A and B synthsised in alcohol solvent. From the DTG results, it can be known that first thermal events at about 100 ^oC is corresponds to removing free water. The second peak at about 300 ^oC is attributed to reactions $H_4TiO_4 \rightarrow 2TiO_2+2H_2O$ and $H_4TiO_3 \rightarrow TiO_2+H_2O$. The thermal weight losses appearing at about 600 ^oC is attributed to the decarboxylation of $BaCO_3$. Ando and Yanagawa et al. proposed that $BaCO_3$ and TiO_2 mixture can be separated into two stages [6]. The first stage is related to the contact area between $BaCO_3$ and TiO_2. Increasing reactants contact points numbers can improve this reaction process. And the second stage is controlled by Ba^{2+} diffusion rate through the $BaTiO_3$ layer forming at the first stage. DTG peaks of sample B between 580 ^oC and 840 ^oC is in good accordance with Ando and Yanagawa whose theory cannot explain the phenomenon of A. There is only one peak at around 620 ^oC in A and weight loss procedure occurs in narrower temperature range between 570 ^oC and 650 ^oC by comparing to B.

Therefore, the reactivity of A is higher than B. Among the two samples, the single step reaction of $BaTiO_3$ is only observed in A and the reaction ending temperature of A is also 190 ^oC lower than B. The single step reaction formation mechanism proposed by T.-T. Lee and Chi-Yuen Huang is more suitable to explain the formation mechanism of A [12]. They used high-energy bead mill to mix ultrafine TiO_2 (8 nm in diameter) and $BaCO_3$ (57 nm in diameter). The lower formation temperature is helpful to produce finer $BaTiO_3$ particles.

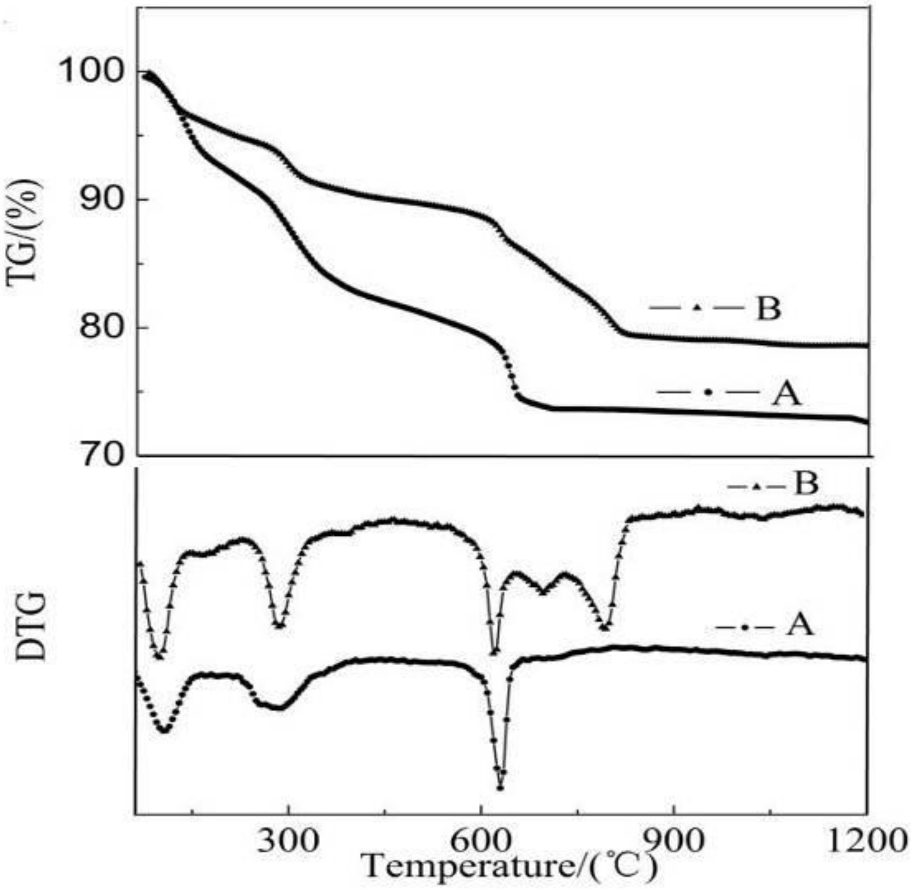

Figure 2. TG-DTG cures of precursors of A and B.

Fig. 3 shows the XRD patterns of A and B obtained for raw and calcined powders of the stoichiometric composition with Ba/Ti=1±0.005. In both precursors of A and B, all the appeared peaks correspond to $BaCO_3$ phase and none TiO_2 crystallites could be found which is in accordance with Petra Pulisová's research [9]. After two hours reaction at 480 ^oC, even though dehydration process of H_4TiO_4 or H_2TiO_3 has finished, there is no evident changes can be observed in the main phases of precursor in A. After two hours reaction at 575 ^oC, the $BaTiO_3$ peaks are detected by XRD in both A and B without the phases of TiO_2. Only trace amount of $BaCO_3$ phase is observed in A but there is relative larger amount of $BaCO_3$ in B at 600 ^oC. From XRD results at 575 ^oC and 600 ^oC, the reaction activity of A is higher than B which is in accordance with the results showed in TG-DTG curves.

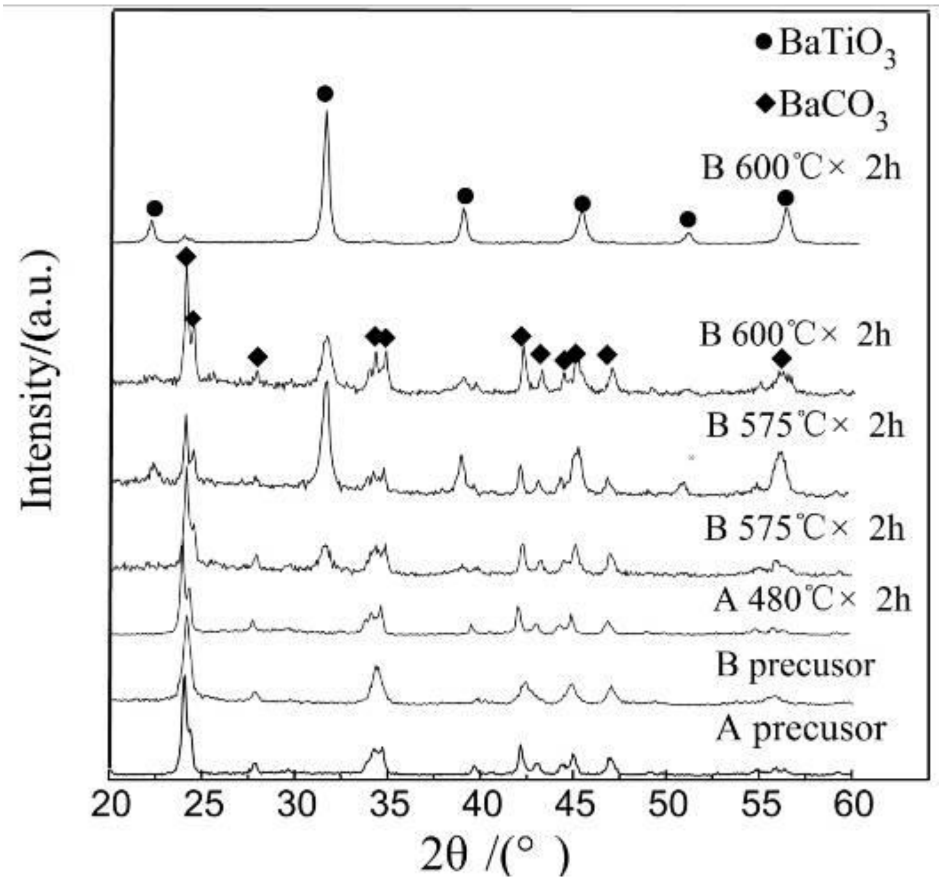

Figure 3. XRD patterns for samples at low temperature range.

3.3. Analysis of phase change

Fig. 4 shows the XRD patterns of A, B calcined at relative high temperature range. At 700 °C thermal insulation for two hours and pure cubic phase of $BaTiO_3$ (JCPDS card: 31-0174) is obtained in A. The Ba_2TiO_4 phase is observed in Fig. 4 and Fig. 5 Raman patterns proving the reaction $BaCO_3 + BaTiO_3 \rightarrow Ba_2TiO_4 + CO_2$ occurred in sample B. And the reaction is also reasons of the second main peaks in DTG curve and low reaction activity of sample B [6]. In general, the XRD patterns of the tetragonal $BaTiO_3$ show split peaks at 45° corresponding to the (h k l) Miller index (002) and (200), whereas cubic $BaTiO_3$ (JCPDS data No. 31-0174) has one single peak at 45° corresponding to (002). At 900 °C the peak between 44° and 46° shows the splitting trend is more obvious in sample A than B. The existence of a not significant degree of tetragonality was evidenced by Raman spectroscopy for its more sensitive pattern on testing small or local tetragonality than XRD[12]. The two samples are characterized as tetragonality for the peaks at 306 and 716 cm^{-1}[13]. The tetragonality of A is larger than B showed in Fig. 4 and Fig. 5 because A precursor transforms into $BaTiO_3$ at lower temperature. Fig. 6 suggests that the tetragonal crystals form and grow with temperature rising in A. Below 700 °C with temperature rising, lattice shrinkage of cubic phase $BaTiO_3$ are reflected by c-axis or a-axis reductions, however at and above 800 °C, increased temperature induces continuous increase tetragonality (minimum 1.005 at 800 °C and maximum 1.010 at 1100 °C) of the nanoparticles. The reason is that the proportion of c-axis inverse to a-axis. In addition, no $BaSO_4$ phases are found in

XRD patterns which indicates that residual SO_4^{2-} have been beyond the testing range of XRD and the content of SO_4^{2-} is less than 0.01% according to ICP results in A.

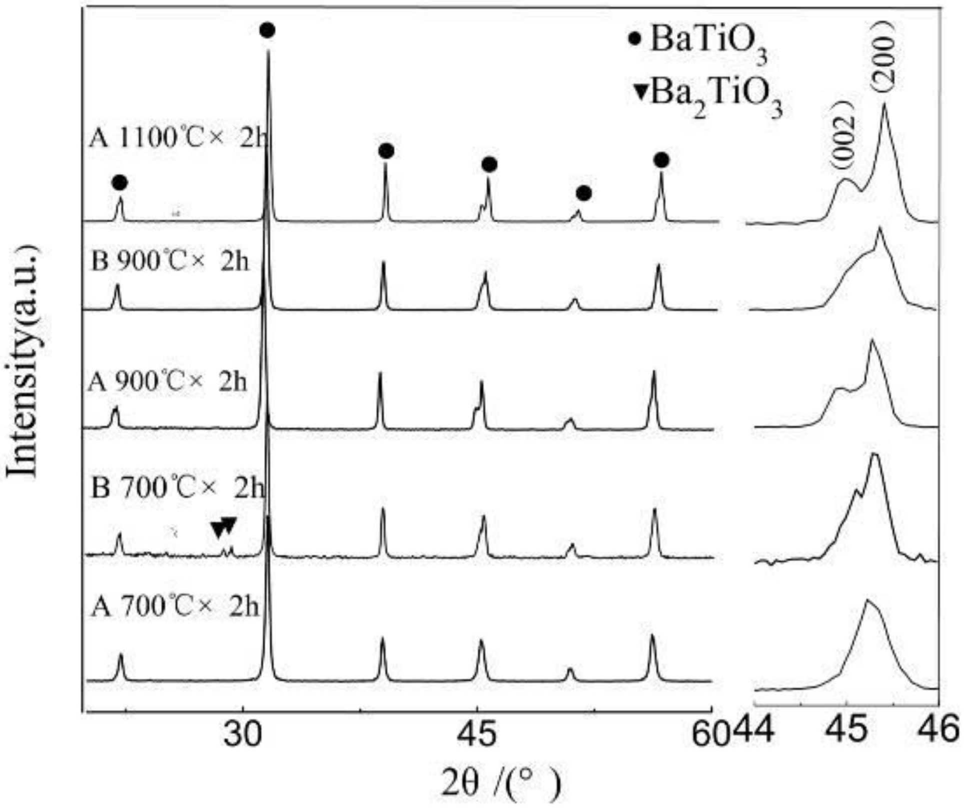

Figure 4. XRD patterns for samples at high temperature range.

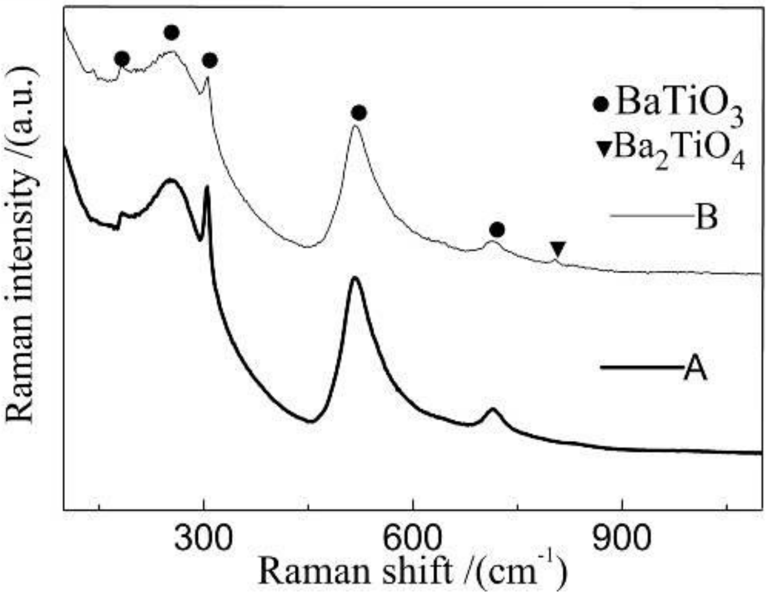

Figure 5. Raman spectra of powders A and B after calcinations at 800 °C for 2 h.

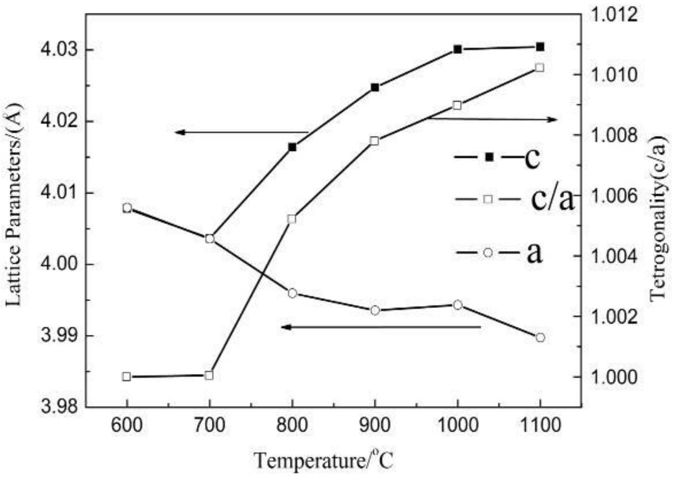

Figure 6. Rietveld analysis results: lattice parameters and tetragonality(c/a) as a function of teperature.

3.3. Analysis of powder microstructure

Fig. 7(a) and (b) shows the SEM graphs of A and B calcined at 700 °C for 2 h. The size distribution of A (d_{50}= 90 nm) is much finer than that of B (d_{50}=170 nm). As mentioned before, thesize of final product $BaTiO_3$ particles depend on the size of raw material TiO_2. H_2TiO_3 with uneven size distribution is prepared by uncontrolled hydrolysis process of $TiOSO_4$ at solvent boiling temperature leading to the occurrence of heterogeneous nucleation. Fig. 7(c) and (d) shows SEM graphs of A, B calcined at 900 °C for two hours. The particles in Fig 7 (c) and (d) grow relative to Fig 7 (a) and (b) for A (d_{50}=160 nm) and B (d_{50}= 450 nm) respectively. Heterogeneous size distribution in B leads to the particles with different specific surface energy. Big ones tend to become larger while small ones become smaller and finally disappear so that the total energy of reaction system becomes lower.

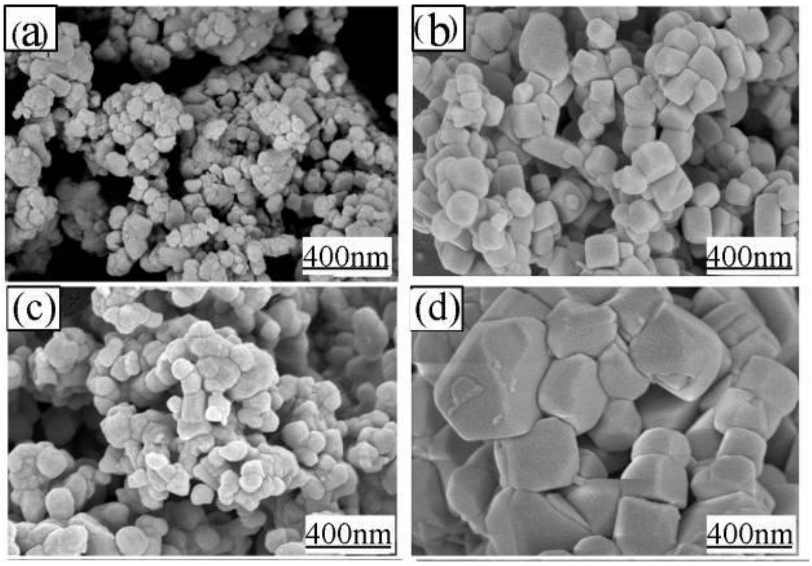

Figure 7. SEM micrographs of the samples annealed for two hours:(a) A at 700 °C, (b) B at 700 °C,(c)A at 900 °C,(d)B at 900 °C.

High reaction temperature promotes phase transition from paraelectric cubic to ferroelectric tetragonal structure at the cost of particles growing reflected by analysis of Fig. 6 and Fig .7. As Fig 7 shows that within low temperature range, particles do not grow remarkable compared with high temperature range, but appearance of tetragonal phase also occurs at high temperature range. In this research no crystal TiO_2 is found during the whole reaction procedure in A and B. But the Ti source in A may have more defects and larger specific surface area after dehydration than Ti source used in B. Therefore, the diffusion rate is higher than traditional solid-reaction method causing $BaTiO_3$ prepared at relative low temperature with fine particles size and uniform size distribution.

3.4. Analysis of dielectric and sintering properties

To study the dielectric properties of materials, sample A powders sintered at 900°C were selected to sinter into ceramics at 1200 °C, 1230 °C, 1260 °C and 1290 °C for two hours. The micrographs in Fig. 8 illustrate the surfaces microstructures of the ceramic samples sintered at different temperature after hot corrosion. Microstructural analysis showed that the $BaTiO_3$ sintering temperature had significant effect on grain size and density. With an increase sintering temperature, the average grain size of ceramic samples increased from 190 nm to 2.3 μm and pore numbers decreased. The results obtained from Table 1 also illustrated that increased sintering temperature promoted sintering densification. The narrow grain size distribution and high density of the ceramics samples is attribute to the fine and uniform size distributions powders. It is well know that fine and uniform particles with high surface energy promote sintering densification by increasing sintering driving force and inhibiting secondary crystallization.

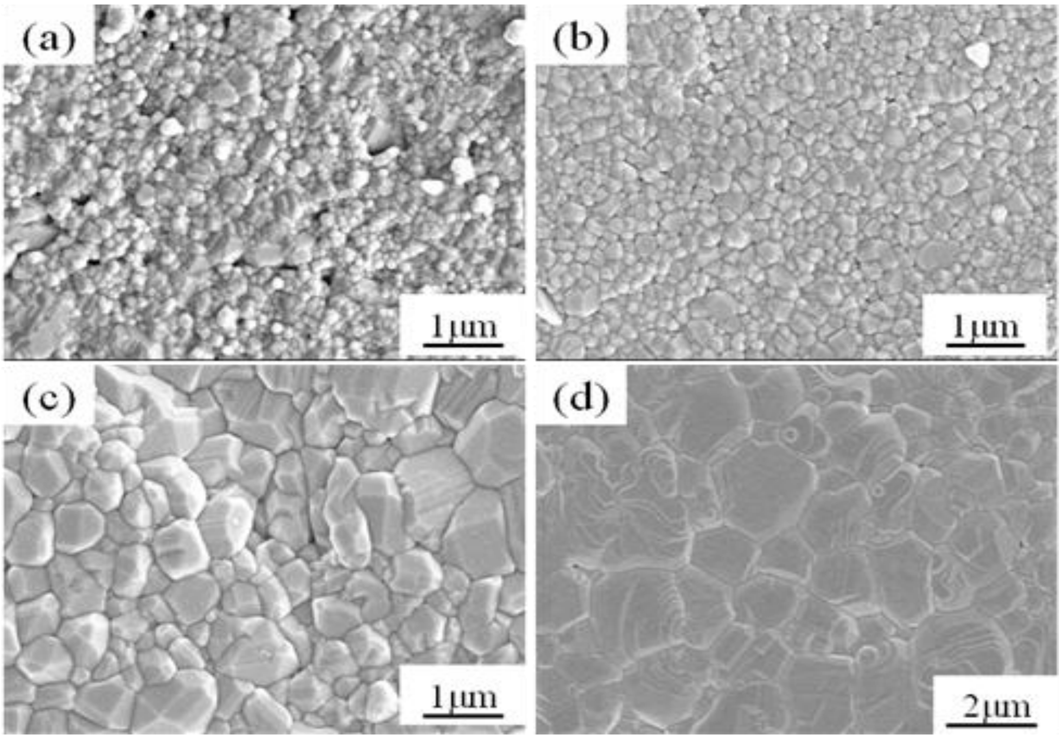

Figure 8. SEM micrographs of the ceramic samples sintered at different temperatures: (a)1200 °C (b) 1230 °C（c）1260 °C（d）1290 °C.

The dielectric properties of the ceramic samples prepared at different temperatures are presented in Table 1 and Figs. 9. The sample sintered at 1260 ◦C shows the highest dielectric constant. The dielectric constant increased with increased sintering temperature under 1260 ◦C but even higher temperature caused deteriorated dielectric performance. It is well known that the density and grain size have great influence on the dielectric properties [14,15]. Cavities can dissipate the energy and deteriorate the dielectric properties. The“grain-size effects” shows when the grain size of $BaTiO_3$ ceramics decreases from 10 to 0.1 μm, the temperature permittivity increases first and then decreases, and maximum permittivity obtains at a grain size of approximately 1 μm [16-19]. The effects of density and grain size have the same trend toward good dielectric properties when sintering temperature under 1260 ^{o}C. The dielectric constant of the sample sintered at 1290 ^{o}C decreased, because effects of density and grain size have adverse trend and grain size effect is dominant. The Curie temperature increased from 121 ^{o}C to 128 ^{o}C when the sintering temperature increased. The grain size is the main effect of Curie temperature [20]. Moreover there is no evidence shows trace amount of Sulfur impurities deteriorated.

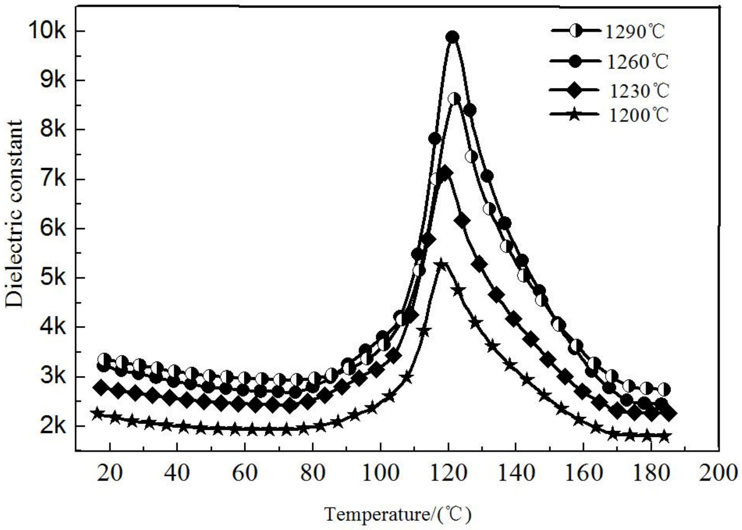

Figure 9. Temperature dependence of dielectric constant for the ceramics.

Table 1. Density, grain size and dielectric properties of the ceramics.

Sinreing temperature	Average grain size	Relative density	Permittivity (25 ^{o}C)	Tanδ (25 ^{o}C)	Curie temperature
1200 ^{o}C	0.19 μm	90.5%	1890	0.031	121 ^{o}C
1230 ^{o}C	0.29 μm	96.1%	2450	0.019	123 ^{o}C
1260 ^{o}C	0.95 μm	97.8%	3250	0.015	126 ^{o}C
1290 ^{o}C	2.70 μm	97.9%	3000	0.016	128 ^{o}C

4. CONCLUSIONS

$TiOSO_4$ can be successfully used to synthesize $BaTiO_3$ under wet chemical mixing method. Neutralized-hydrolysis product of $TiOSO_4$ shows more superiorities than self-hydrolysis product on synthesizing finer $BaTiO_3$ at relative low temperature range with high tetragonality. Alcohol in solvent plays a role in inhibiting $BaCO_3$ particles growth thus promotes getting homogeneous precursors. Because the reaction mechanisms is different Great sintering capability of powders synthesized at 900 ^oC is obtained, which shows high density(97.8%) at 1260 ^oC with two hours calcining .The permittivity of ceramic can reach 3200 at room temperature and 9500 at 126 ^oC using $BaTiO_3$ powers synthesized at 900 ^oC. No evidence reveals that the trace amount residual SO_4^{2-} deteriorate the permittivity.

References

1. A. Beauger, J. Mutin and J Niepce J, *J. Mater. Sci.*, 18 (1983) 3041-3046.
2. C.Gomez-Yanez, C.Benitez and H. Balmori-Ramirez, *Ceram. Int.*, 26 (2000) 271-277.
3. T.T. Lee, C.Y. Huang, C.Y Chang, IK. Cheng, C.T Hu and C.T Lee, *J. Mater Res*., 27 (2012) 2495-2502.
4. D.F.K. Hennings, B.S Schreinemacher and H. Schreinemacher, *J. Am. Ceram Soc*., 84 (2001), 2777-2782.
5. H.I. Hsiang, Y.L. Chang, J.S. Fang and F.S. Yen, *J. Alloy. Compd*., 509 (2011) 7632-7638.
6. C. Ando, R. Yanagawa, H. Chazono, H. Kishi and M. Senna. J. *Mater Res*., 19 (2004) 3592-3599.
7. C. Pithan, D. Hennings and R. Waser, *Int. J. Appl. Ceram. Tec*., 2 (2005) 1-14.
8. J. Krysa, M. Keppert, J. Jirkovsky, V. Stengl and J. Subrt, *Mater Chem Phys*., 86 (2004) 333-339.
9. P. Pulisova, J. Bohacek, J. Subrt, L. Szatmary, P. Bezdicka and N. Murafa, *Catal Today*., 161 (2011) 84-90.
10. P.E.Tsakiridis, P. Oustadakis, A. Katsiapi, M. Perraki and S. Agatzini, *J Hazard Mater*., 194 (2011) 42-47.
11. S.S Ryu, D.H.Yoon, *J Mater Sci*., 42 (2007) 7093-7099.
12. F.A. Rabuffetti, R.L. Brutchey, *J. Am. Ceram Soc*., 134 (2012) 9475-9487.
13. U.D. Venkateswaran, V.M. Naik and R. Naik, *Phys Rev B.*, 58 (1998) 14256-14260.
14. N. Ma, B.P. Zhang , W.G. Yang and D. Guo, *J Eur Ceram Soc.*, 32 (2012) 1059-1066.
15. M.H. Frey, D.A. Payne, *Physical Review B*., 54 (1996) 3158-3168.
16. L. Gao, X.L. Liu, J.Q. Zhang, S.Q. Wang and J.F. Chen, *Mater Chem Phys*., 88 (2004) 27-31.
17. Z. Zhao, V. Buscaglia and M. Viviani, *Phys Rev B*., 70 (2004) 1-8.
18. Y.S. Tian, Y.S. Gong; Z.L. Zhang and D.W. Meng, *J. Mater. Sci*., 12 (2014) 5467-5474.
19. Y. Tao, Z.G. Sheng and W.W. Zhang, *Mater Chem Phys*., 98 (2006) 450-455.
20. B.D. Begg, K.S. Finnie and E.R. Vance, *J. Am. Ceram Soc*., 79 (1996) 2666-2672.